Fluorinated Photodynamic Therapy Device Tips and their Resistance to Fouling for *In Vivo* Sensitizer Release

Ashwini A. Ghogare[1], Joann M. Miller[2], Bikash Mondal[3], Alan M. Lyons[3], Keith A. Cengel[2], Theresa M. Busch[2]* and Alexander Greer[1]*

[1]Department of Chemistry and Graduate Center, Brooklyn College, City University of New York, Brooklyn, NY
[2]Department of Radiation Oncology, University of Pennsylvania, Philadelphia, PA
[3]Department of Chemistry and Graduate Center, College of Staten Island, City University of New York, Staten Island, NY

ABSTRACT

We describe progress on a one-step photodynamic therapy (PDT) technique that is simple: device tip delivery of sensitizer, oxygen and light simultaneously. Control is essential for their delivery to target sites to generate singlet oxygen. One potential problem is the silica device tip may suffer from biomaterial fouling and the pace of sensitizer photorelease is slowed. Here, we have used biomaterial (*e.g.* proteins, cells, *etc.*) from SQ20B head and neck tumors and whole blood for an assessment of fouling of the silica tips by adsorption. It was shown that by exchanging the native silica tip for a fluorinated tip, a better nonstick property led to an increased sensitizer output by ~10%. The fluorinated tip gave a sigmoidal photorelease where singlet oxygen is stabilized to physical quenching, whereas the native silica tip with unprotected SiO–H groups gave a slower (pseudolinear) photorelease. A further benefit from fluorinated silica is that 15% less biomaterial adheres to its surface compared to native silica based on a bicinchoninic acid assay (BCA) and X-ray photoelectron spectroscopy (XPS) measurements. We discuss how the fluorination of the device tip increases biofouling resistance and can contribute to a new pointsource PDT tool.

INTRODUCTION

Treatment of tumors by photodynamic therapy (PDT) is a two-step process that involves the delivery of the photosensitizer to a patient followed by local illumination with a sensitizer-exciting wavelength of light (1–3). The development of a one-step process for local delivery of sensitizer, oxygen and illumination would simplify the application of PDT, increasing the ease of its use and potentially expanding its clinical utility.

Contrary to pointsource (PDT) that uses a systemically administered sensitizer, a technique being developed is PDT (4). Pointsource PDT is a medical device with a photocleavable sensitizer group to assemble all components for PDT at a specific site. Figure 1 shows the pointsource PDT technique; it delivers sensitizer, light and oxygen as precursors to singlet oxygen (a cytotoxic excited state of O_2). The sensitizer photorelease is based on a dioxetane cleavage process (5–12).

Thus far, pointsource PDT was shown to produce a highly defined killing radius of glioma U87 (4) and OVCAR-5 cancer cells *in vitro* (13). This observation raises key questions about limitations of pointsource PDT that have not yet been addressed. Does the device tip biofoul? Would biofouling be expected to arise during the time course of a typical PDT session? Do cells adhere to the tip and impede sensitizer photorelease? Does fluorination of the tip increase biofouling resistance in the pointsource PDT technique?

Proteins, cells or microorganisms, in this manuscript called "biomaterial", are known to adhere to surfaces, such as hydrophilic silica (14,15), but less to hydrophobic fluorinated silica (16). Indeed, polymers have been developed that have anti-biofouling coatings, such as fluoropolymers and poly(ethylene glycol) (PEG) polymers (17–19). Some surfaces offer *added* biofouling protection by the production of reactive oxygen species (ROS). A vanadium pentoxide nanoparticle surface as a haloperoxidase mimic is known to produce singlet oxygen and resist biofouling (20). A porphyrin-modified film that produced $^1O_2$ was found to have antibacterial activity (21) and anti-biofouling activity (22). Similarly, silica/polydopamine/silver nanoparticle (23), copper iodide nylon (24) and electrochemical surfaces (25), which produced ROS were found to resist biofouling. A self-cleaning superhydrophobic surface containing TiO_2 nanoparticles was also found to photooxidize bovine serum albumin (26).

Thus, our hypothesis was that inhibition of sensitizer release in pointsource PDT will scale with biomaterial adsorption on the device tip. We had also tested the hypothesis that sensitizer turn-out levels will be better maintained based on the presence of a fluorosilane coating (tip **1**) compared to the native silica surface (tip **5**). We have analyzed whether surface biomaterial fouling limits tip output of sensitizer in pointsource PDT.

We report here on the biofouling of pointsource PDT device tips tested after placing the tip in contact with the surface of a surgically exposed flank tumor (SQ20B tumors in nude mice). Figure 2 shows an image of the device tip placed on the exposed tumor surface. In other experiments, device tips were soaked in whole blood as a phantom body fluid. Overlapping chromophores make the delivery of sensitizer into the tumor or blood samples difficult to quantitate. For this reason, fouling effects of the device tips were quantitated by a sensitizer photorelease inhibition analysis. Data were also collected with a bicinchoninic
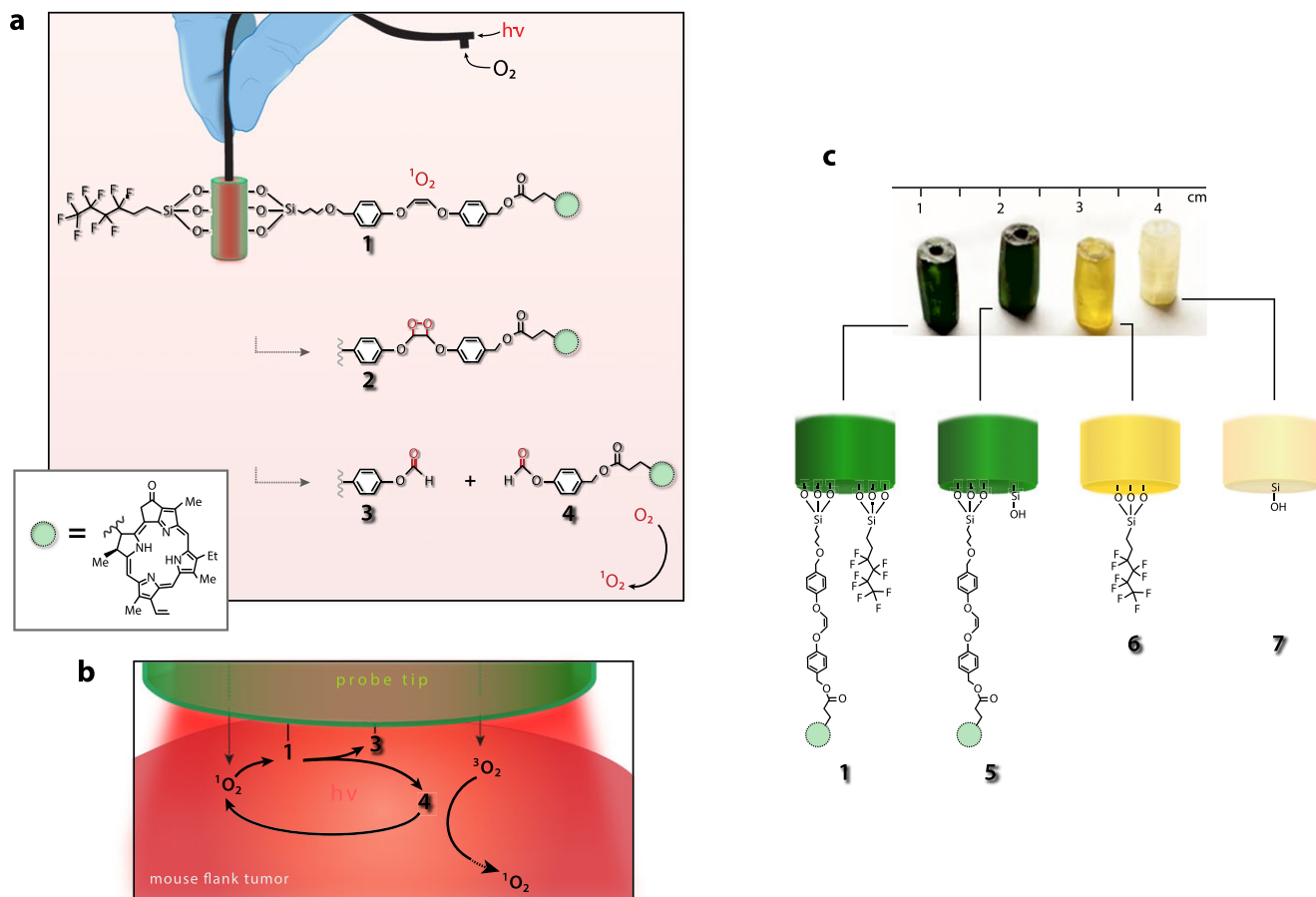
Figure 1. Schematic presentation of the pointsource PDT technique with various device tips. (a) Diode laser light and O_2 gas are passed through a hollow fiber optic and emerge through the silica tip that is functionalized by a sensitizersilane and/or fluorosilane outer layer. An inset on the left shows the sensitizer structure. (b) The proposed mechanism is shown summarizing the steps in the sensitizer release system of tip **1**. Much of the laser light is distributed out of the end of the tip. The device tip leaves behind the sensitizer upon conversion of the ethene to a dioxetane **3** and *additional* $^1O_2$ is generated away from the tip. (c) Shown is a photograph of four device tips [sized 5×10 mm^2 ($d \times l$)] and chemical drawings of the bottom of tips with the anchored groups or silanol.

acid assay (BCA) and X-ray photoelectron spectroscopy (XPS) to quantitate the amount of biomaterial (*e.g.* proteins, cells, *etc.*) adsorbed on "dummy" tips **6** and **7**, which contained no sensitizer. The results not only show that tip **1** biofouls by ~8%, based on experiments in the presence and absence of biomaterial, but retains a rapid sigmoidal release feature indicative of an autocatalytic mechanism.

MATERIALS AND METHODS

Device fabrication. A fiber optic device with silica device tips **1** and **5** was used as described previously (4,5). Briefly, pieces of silica were fluorinated by soaking in 1×10^{-3} M 3,3,4,4,5,5,6,6,6 nonafluorohexyltrimethoxysilane and then refluxed in toluene for 24 h. Any nonafluorosilane that was not covalently attached to the silica surface was washed away by Soxhlet extraction in methanol for 24 h.

Tumor model. Cells of SQ20B head and neck squamous cell carcinoma (ATCC, Manassas, VA) were cultured in DMEM medium (ATCC) supplemented with 10% fetal bovine serum (Gibco, Carlsbad, CA), 2 mM L-glutamine (Gibco), 100 units mL^{-1} penicillin (Gibco), 100 μg mL^{-1} streptomycin (Gibco) and maintained in a humidified atmosphere with 5% CO_2 at 37°C. Cells in log phase were harvested, and resuspended at 2×10^7 cells mL^{-1} in a 1:1 solution of phenol red-free matrigel basement membrane matrix (BD Biosciences, San Jose, CA) and normal saline (27–29). Each 8–9-week-old female athymic nude mouse (Charles River Laboratories in Frederick, MD) was inoculated with 1×10^6

SQ20B cells intradermally on the right and left flank of the mouse. The tumor suspension was in 50% matrigel. Animals were used for experiments 2 weeks after tumor inoculation when the intradermal tumors reached volumes of ~50–150 mm^3. The mice were anesthetized by inhalation of isoflurane in medical air delivered through a nosecone (VetEquip anesthesia machine, Pleasanton, CA). An incision was made adjacent to the flank tumor and a skin flap was created to expose the tumor. A device tip (**1** or **5–7**) was placed on the tumor surface for 1 h. Once the device tip was in contact with the tumor, two drops of saline solution were applied to the exposed area to prevent dehydration of the tissue and its adhesion. After treatment, the device tips were removed and preserved in dry ice for further analysis.

Sensitizer photorelease studies. The bottom face of tips **1, 5–7** were placed (1) on the surgically exposed surface of a SQ20B tumor grown intradermally on the flank of athymic nude mouse, or (2) in 100 μL whole blood obtained from Sprague-Dawley rats (37 °C). The tips were placed for 1 h on the tumor or in blood either (1) in the dark or (2) with 669 nm laser irradiation via hollow fiber optic coupling with oxygen flowing through the tip. The tips were then rinsed with 5 mL saline and analyzed for subsequent sensitizer photorelease (attached to the device) from the tips into 1 mL *n*-butanol, quantified by monitoring the Q-band ($\lambda = 663$ nm) with UV–VIS spectroscopy (6). After photorelease in *n*-butanol, the device tips were subjected to Soxhlet extraction with methanol at 68–70°C for 24 h, thereby removing any adsorbed sensitizer, and then subjected to a previously described hydrofluoric acid stripping method (5) to determine the amount of sensitizer bound to the surface. Treatments were at a fluence rate of 51–550 mW cm^{-2} over a period of 0–2 h.
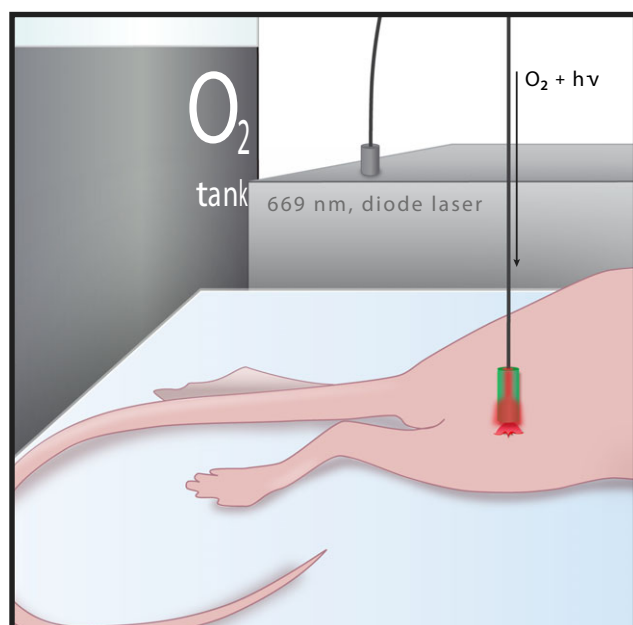
Figure 2. A schematic of the cylindrical device tip held vertically, in contact with a surgically exposed flank tumor of a nude mouse. Red laser light and oxygen gas travel through the hollow fiber optic. Sensitizer, light, $^3O_2$ and $^1O_2$ emerge out of the device tip

BCA studies. After exposing the front face of device tips to the SQ20B tumor or the Sprague–Dawley rat blood, the tips were washed with 5 mL saline and the adsorbed biomaterial was stripped off with 200 µL 20% (*v/v*) Solvable™ in 1 mL 1% SDS solution. The amount of biomaterial adsorbed on the device tips, as µg, was determined using BCA assay in comparison to the calibration curve of standard protein albumin (30,31). Experiments were carried out two or more times. From the plot, 10 µL blood has 876 ± 20 µg protein. The compatibility of BCA assay in 20% (*v/v*) Solvable™ in 1 mL 1% SDS solution for detection of proteins in blood was validated by using different volumes of blood.

X-ray photoelectron spectroscopy studies. The flat front faces of tips were placed in 100 µL whole blood obtained from Sprague–Dawley rats for various lengths of time at 37°C. After exposing the device tips to the blood, the tips were washed with 5 mL saline and dried using a high vacuum freeze dryer lyophilizer. The amount of protein adsorbed on glass samples was analyzed with XPS using an Omicron Nanotechnology system equipped with an Al Kα X-ray source (1486.6 eV). A hemispherical analyzer (EA-125) was operated in constant analyzer energy (CAE) mode and equipped with one channel electron multiplier to measure the binding energies of the emitted photoelectrons. XPS spectra were collected under ultra-high vacuum ($<1 \times 10^{-8}$ torr) with high resolution scans (0.5 eV step size) over the range of binding energy (from 600 to

0 eV) to cover N 1s (~400 eV), O 1s (~532.8 eV) and C 1s-2p (~285–290 eV), for signals typical of absorbed protein (32). Surface areas with a diameter less than 1.5 mm were analyzed and referenced by setting C 1s peak to 284.8 eV to compensate for residual charging. Finally, the peak area ratios of N 1s/Si 2p, C 1s/N 1s and C 1s/Si 2p were calculated to compare the amount of adsorbed protein on the silica surfaces (33).

RESULTS

Studies were performed on device tips that were biofouled through exposure to one of two types of media (mouse flank tumor and rat whole blood). The effects of biofouling on sensitizer photorelease were evaluated. After biofouling effects are established, repellent materials could be further developed (34–40) as more effective pointsource PDT device tips.

Effects of biofouling on device tip sensitizer release

Initially, we conducted experiments to quantitate biofouling of the device tip by contact with SQ20B tumors. Sensitizer photorelease inhibition—which can occur from the adhering of tumor biomaterial—was used as evidence for device tip biofouling.

Table 1 shows that exposing the tip to SQ20B tumor affects the yield of sensitizer photorelease. When exposed to tumor for 2 h in the dark, Table 1 (entries 1 and 5, and 2 and 6) show a 8% reduction in tip **1**, and a 18% reduction in tip **5**. The inhibition of sensitizer **4** photoreleased was lower for fluorinated tip **1** compared to the native tip **5** (~10%). We found that the reduction in amount of sensitizer released was similar for tips biofouled with tumor and with blood (Table 1, compare entries 1 with 3, and 2 with 4). The tips were then dissolved by hydrofluoric acid and show that 5–8% of sensitizer remained bound to the surface, which indicates that the tips were comparable since all were near depleted of sensitizer.

Figure 3 shows the time course of sensitizer photorelease from device tips **1** and **5** *after* exposure to the tumor or whole blood. That is, the photorelease in *n*-butanol was carried out after the tip had been in contact with biological media. Fluorinated tip **1** gave a sigmoidal photorelease, whereas the native silica tip **5** gave a slower (pseudolinear) photorelease. Furthermore, the amount of sensitizer adsorbed to tip **1** was three times less compared to tip **5** as revealed by Soxhlet extraction with methanol at 68–70°C for 24 h, to detach any adsorbed sensitizer. After the covalent ethene bridge bonding the sensitizer to the surface is broken, the amount of sensitizer **4** adsorbed to tip **1** was ~17% (35 nmol) and to tip **5** was ~54% (11 nmol). The tip fouling

Table 1. Tumor- or blood-contact dependence of the photorelease of sensitizer **4** from device tips **1** and **5** into *n*-butanol.*

Entry	Device tip	Test medium	% Photoreleased sensitizer **4**	% Adsorbed sensitizer on tip[†]	% Covalently-bound sensitizer remaining on tip[‡]
1	**1**	Tumor	77 ± 2	17 ± 5	6 ± 2
2	**5**		40 ± 2	53 ± 5	7 ± 3
3	**1**	Blood	79 ± 2	16 ± 5	5 ± 2
4	**5**		38 ± 3	55 ± 5	7 ± 4
5	**1**	None	85 ± 2	9 ± 3	6 ± 5
6	**5**		58 ± 3	34 ± 5	8 ± 4

*The device tip was placed in contact with the surgically exposed tumor or whole blood for 1 h. The photorelease in *n*-butanol was then carried out after the tip had been in biological contact. The tip was affixed to the hollow optical fiber, delivering O_2 and 669 nm laser light through the tip (irradiance = 51–550 mW cm^{-2}, time = 0–2 h) and the amount of **4** released determined after 1 h. [†]The amount of **4** adsorbed on the tip was determined by Soxhlet extraction with methanol at ~70°C for 24 h. [‡]The last remaining covalently bound sensitizer was quantified by removal with HF and analysis of the Q-band (λ = 663 nm) of the sensitizer by UV–VIS spectroscopy judged against a prior constructed calibration curve of the sensitizer. Experiments were carried out three or more times and the error limits are expressed as standard deviation (SD).
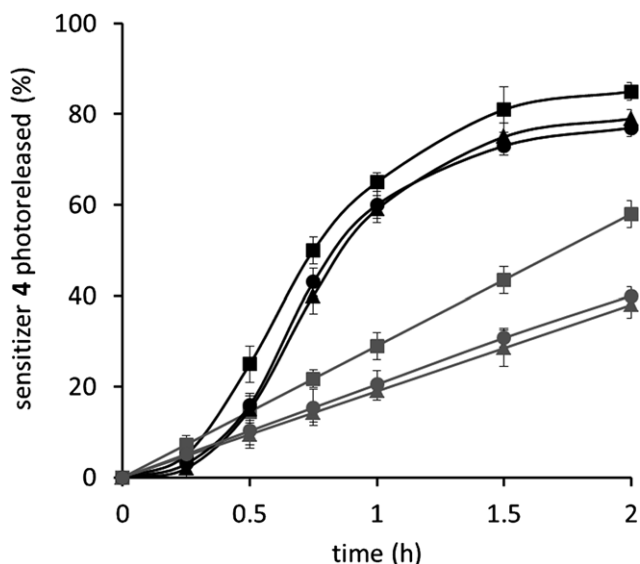
Figure 3. The percent of sensitizer **4** photoreleased free from device tip **1** (dark line) and tip **5** (light line) in 1 mL *n*-butanol. The tips were pre-exposed for 1 h to: (1) mouse flank tumor through an incision (●), (2) whole blood (▲), and (3) *n*-butanol (■). The concentration of sensitizer **4** was measured by UV–VIS following the sensitizer Q-band at $\lambda = 663$ nm.
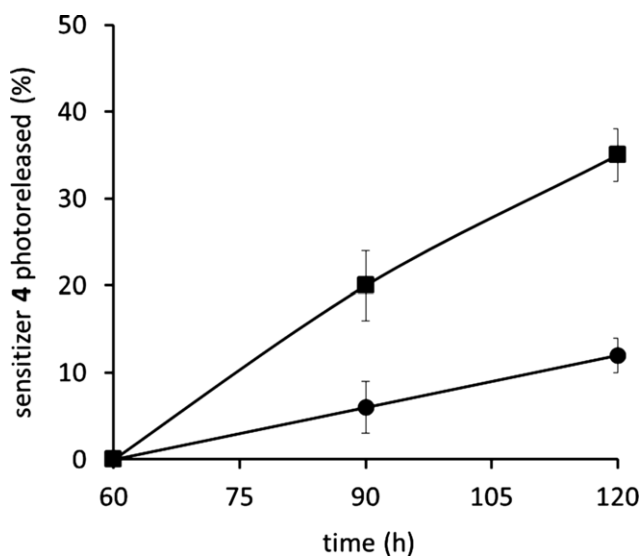
Table 2. Blood and tumor cell adsorption to fluorinated silica **6** and native silica **7** surfaces.*

	Cell quantities adsorbed on device tips (µg)			
	Whole blood[†]		SQ20B tumor[†]	
Time	Fluorinated tip **6**	Native tip **7**	Fluorinated tip **6**	Native tip **7**
6 min	85 ± 4	102 ± 5	–	–
15 min	90 ± 5	105 ± 3	–	–
0.5 h	100 ± 3	115 ± 3	–	–
1 h	105 ± 3	125 ± 8	35 ± 8	58 ± 7
3 h	127 ± 3	140 ± 5	–	–
10 h	198 ± 8	201 ± 5	–	–

*Device tips were pre-exposed to rat blood (100 µL) for 1 h. Error bounds were obtained from two or more measurements and are expressed as standard deviation (SD). [†]Adsorbed tumor or blood cells were stripped off by Solvable™ and quantitated by a BCA assay.
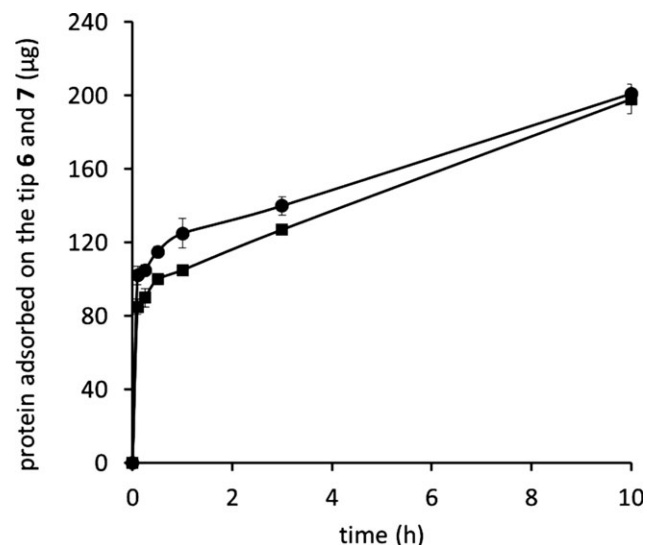

Figure 4. A plot of remaining sensitizer **4** photoreleased into *n*-butanol *vs* time for tip **1** (■) and tip **5** (●). These points were collected after the tips already used for **4** photorelease in a mouse flank tumor for 1 h.

Figure 5. A plot of blood cells adsorbed to tip **6** (■) and tip **7** (●) *vs* time when immersed in blood. The quantity of protein was determined by a BCA assay after stripping with a Solvable™ solution.

Effect of adsorption of cellular material

The data show that biomaterial (*e.g.* proteins, cells, *etc.*) from the SQ20B tumors and rat blood adsorb onto the tip surfaces. The amount of this biofouling on both the fluorinated silica **6** and native silica **7** surfaces was determined based on a BCA assay and XPS measurements.

Table 2 and Fig. 5 show the BCA assay results and the amount of biomaterial residue adhering to tips **6** and **7**. A ~15% higher adsorption was observed on the native silica **7** compared to the fluorinated silica **6**. In the first 5 min, there is a rapid adsorption (85 µg for **6**; 102 µg for **7**). After the biofouling increases sharply during the first 5 min, it slows to 2 h and continues for 10 h. The rate of biomaterial adsorption onto the silica surfaces remains constant from ~1 to 10 h.

Figure 6 shows an XPS analysis of the adsorption of biomaterial from blood on tip **6**. The ratio of the N 1s to Si 2p and C 2s to Si 2p peaks were used to determine the relative amount of

experiments conducted with the tumors and blood are consistent with each other and complementary.

Similar to Fig. 3, Fig. 4 also shows the time course of sensitizer photorelease from device tips **1** and **5**. The difference between Figs. 3 and 4 is that the latter was collected with the tip placed on the SQ20B tumor with light and oxygen purging through it for 1 h (amount of sensitizer delivered to tumor: 15% for tip **1** and 3% for tip **5**). Once placed in *n*-butanol, Fig. 4 shows the fluorinated tip **1** released significantly more sensitizer (35%) than the native tip **5** (12%). That is, sigmoidal release was not observed since the recording of sensitizer departure started at time = 1 h, not at time = 0 h.

protein and other biological materials on the surface. During the first hour of immersion, the amount of biomaterial adsorbed on the surface increases rapidly with time. The C 1s to N 1s ratio remains constant throughout this period, indicating that C and N adsorption rates are similar. This rapid initial adsorption of biomaterials is consistent with the adsorption isotherm of protein studied on various surfaces (41).

After 1 h of immersion, however, the N 1s/Si 2p ratio remains relatively constant (Fig. 6). This apparent stability may be due to the formation of a complete biomaterial coating on the silica tip after 1 h of immersion. This layer is sufficiently thick to completely cover the underlying silica, preventing detection of Si 2p peaks in the XPS spectrum, as shown in Fig. 7. The N 1s (~400 eV) signal is characteristic of adsorbed biomaterial at the surface (42,43). Peak area ratio of N 1s/Si 2p, C 1s/N 1s and C 1s/Si 2p were compared to eliminate any variation between different XPS samples (44,45). Accumulation of biomaterial does continue, as shown in Fig. 5 for the BCA assay results. However, thicker layers of biomaterial would not be distinguished by XPS due to the limited penetration depth (5–30 nm) of the escaping electrons. Thus, once a sufficiently thick layer of bio-
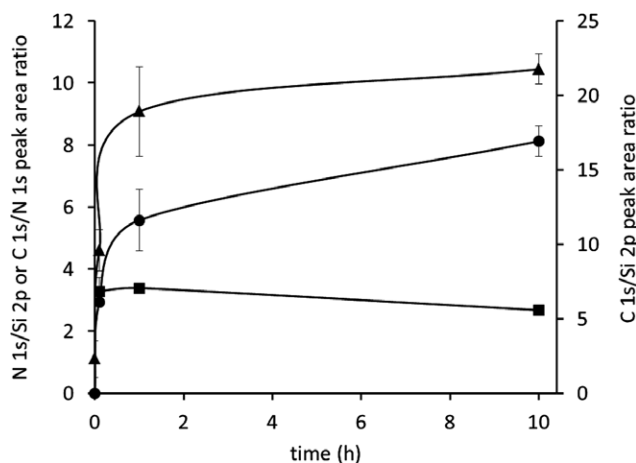

Figure 6. Time profile for XPS peak area ratio changes of C 1s/Si 2p (▲), N 1s/Si 2p (●), and C 1s/N 1s (■) of tip **6** immersed in whole blood.
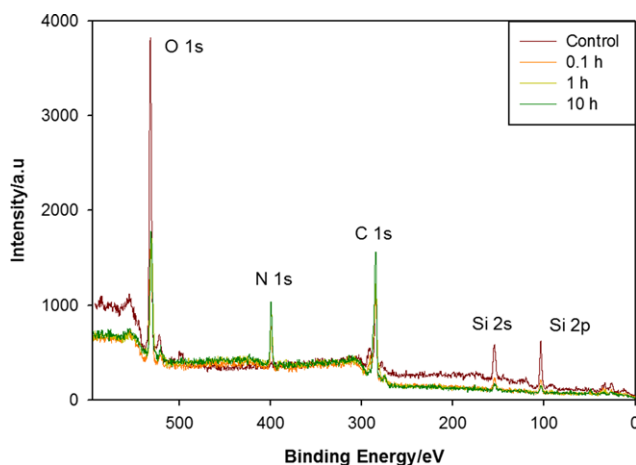

Figure 7. X-ray photoelectron spectroscopy spectra of clean silica **6** and silica **6** contaminated by whole blood.

material is deposited on the silica surface to obscure the Si 2p peak, XPS cannot be used to detect further biomaterial accumulation.

DISCUSSION

Some details are now available on how pointsource PDT device tips **1** and **5** are fouled. Tip fouling experiments were carried out where SQ20B tumors and whole blood showed sensitizer release inhibition of ~6% for **1** and ~10% for **5** after 1 h. Thus, the hydrophobicity of the fluorinated tip provides some protection against biofouling. Figure 3 shows sigmoidal release behavior of **4** for tip **1** that is attributed to an autocatalytic process (6), where surface fouling does not significantly inhibit the release of sensitizer.

We now know that tip fouling was minimal because of the sensitizer turnout levels that were maintained. Thus, fouling is not expected to be problematic over the time course of a typical PDT session; furthermore, the tips are intended to be replaced after each treatment. This is an important criterion to have met due to the sensitizer delivery feature of the pointsource PDT strategy (4). We demonstrate that ~15% less biomaterial adheres to the fluorinated silica than to native silica. The BCA assay shows a constant increase in biomaterial from 1 to 10 h, whereas the XPS shows that the level after 1 h remains constant. This is because once a complete and sufficiently thick layer of biomaterial forms on the silica surface, the underlying Si can no longer be seen by the XPS instrument. It makes sense that when silica is treated with nonafluorosilane the fraction of silicon observable on the surface by XPS at time = 0 (before protein adsorption) is smaller than native silica. The fluorinated silica surface does adhere proteins and cells—just less than the native silica surface due to the residual charges on the untreated silica. Bacteria could be present as a foulant, although there are more cells present than bacteria. Our work did not examine whether the adsorption of biomaterial is due to a hydrophobic and electrostatic interactions (46–48), or other mechanisms.

Lastly, we now know there is a complimentary effect where the fluorinated tip **1** not only repels biofoulants better, it also suppresses surface $^1O_2$ physical quenching (5–7) for a more efficient sensitizer photorelease. It could be argued that added biofouling protection results from the production of $^1O_2$ at the surface of tips **1** and **5** as has been observed for other surfaces which produce $^1O_2$ or ROS (20–26). We believe that generation of $^1O_2$ on (or near) the tip will retard and/or prevent fouling on/ near that surface. The magnitude of this effect will depend on several factors. If sufficient $^1O_2$ is generated in an environment with low amounts of proteins, cells, microorganisms, *etc.* then biofouling might, indeed, be prevented. However, in an environment rich in proteins, cells, *etc.*, then the $^1O_2$ production rate would need to be sufficiently high to overcome the loading of biomaterial that could react with $^1O_2$. Each cell, bacterium or protein could consume many $^1O_2$ molecules. Other studies (49–51) have examined the reaction of $^1O_2$ with biological media that produce peroxides, which can decompose and/or chemiluminesce (52–56).

CONCLUSION

There is still much research to be done before pointsource PDT can be used clinically. Data obtained from the tumor and blood

fouling studies described here will contribute to the ongoing development of pointsource PDT (4). The pointsource PDT device tip was modified with nonafluorosilane to improve its protection against biofouling. The fluorinated tip led to improved biofouling resistance based on sensitizer photorelease performance.

Future studies could continue to resolve outstanding questions concerning a one-step PDT process (*i.e.* simultaneous delivery of sensitizer, oxygen and light) to simplify the application of PDT. Other device configurations could be beneficial. Advantages may exist for micropillar roughened device tips, such as 3D-printed superhydrophobic surfaces, which reduce the contact between the tip and tissue (57,58). Device tips could also be designed with different sensitizer types (59–65) to customize delivery based on tumor type (66–68). Finally, research efforts could seek advantages for *intraoperative* use of pointsource PDT for precision treatment of residual disease. Research efforts are in progress in these directions.

REFERENCES

1. Kessel, D. and T. H. Foster (Eds) (2007) Symposium-in-print: Photodynamic therapy. *Photochem. Photobiol.* **83**, 995–1282.
2. Singlet oxygen: Applications in biosciences and nanosciences (Edited by S. Nonell and C. Flors), pp. 1–450. Royal Society of Chemistry (RSC), Abingdon, Oxfordshire, UK (2015).
3. Li, B. and B. C. Wilson (2015) Introduction to the special issue on photodynamic therapy. *J. Innov. Opt. Health Sci.* **8**, 1502001–1502003.
4. Ghogare, A., I. Rizvi, T. Hasan and A. Greer (2014) Pointsource delivery of a photosensitizer drug and singlet oxygen: Eradication of glioma cells in vitro. *Photochem. Photobiol.* **90**, 1119–1125.
5. Bartusik, D., D. Aebisher, G. Ghosh, M. Minnis and A. Greer (2012) Fluorine end-capped optical fibers for photosensitizer release and singlet oxygen production. *J. Org. Chem.* **77**, 4557–4565.
6. Bartusik, D., M. Minnis, G. Ghosh and A. Greer (2013) Autocatalytic-assisted photorelease of a sensitizer drug bound to a silica support. *J. Org. Chem.* **78**, 8537–8544.
7. Ghosh, G., M. Minnis, A. A. Ghogare, K. A. Cengel, T. M. Busch and A. Greer (2015) Photoactive fluoropolymer surfaces that release sensitizer drug molecules. *J. Phys. Chem. B* **119**, 4155–4164.
8. Hossion, A. M. L., M. Bio, G. Nkepang, S. G. Awuah and Y. You (2012) Visible light controlled release of anticancer drug through double activation of prodrug. *ACS Med. Chem. Lett.* **4**, 124–127.
9. Bio, M., P. Rajaputra, G. Nkepang, S. G. Awuah, A. M. L. Hossion and Y. You (2013) Site-specific and far-red-light-activatable prodrug of combretastatin A-4 using photo-unclick chemistry. *J. Med. Chem.* **56**, 3936–3942.
10. Gorka, A. P., R. R. Nani, J. Zhu, S. Mackem and M. J. Schnermann (2014) A near-IR uncaging strategy based on cyanine photochemistry. *J. Am. Chem. Soc.* **136**, 14153–14159.
11. Gorka, A. P., R. R. Nani and M. J. Schnermann (2015) Cyanine polyene reactivity: Scope and biomedical applications. *Org. Biomol. Chem.* **13**, 7584–7598.
12. Klán, P., T. Šolomek, C. G. Bochet, A. Blanc, R. Givens, M. Rubina, V. Popik, A. Kostikov and J. Wirz (2013) Photoremovable protecting groups in chemistry and biology: Reaction mechanisms and efficacy. *Chem. Rev.* **113**, 119–191.
13. Bartusik, D., D. Aebisher, A. Ghogare, G. Ghosh, I. Abramova, T. Hasan and A. Greer (2013) A fiberoptic (photodynamic therapy type) device with a photosensitizer and singlet oxygen delivery probe tip for ovarian cancer cell killing. *Photochem. Photobiol.* **89**, 936–941.
14. Pohl, J., I. Saltsman, A. Mahammed, Z. Gross and B. Röder (2015) Inhibition of green algae growth by corrole-based photosensitizers. *J. Appl. Microbiol.* **118**, 305–312.
15. Roy, I., P. Kumar, R. Kumar, T. Y. Ohulchanskyy, K.-T. Yong and P. N. Prasad (2014) Ormosil nanoparticles as a sustained-release drug delivery vehicle. *RSC Adv.* **4**, 53498–53504.
16. Costacurta, S., P. Falcaro, L. Malfatti, D. Marongiu, B. Marmiroli, F. Cacho-Nerin, H. Amenitsch, N. Kirkby and P. Innocenzi (2011) Shaping mesoporous films using dewetting on X-ray pre-patterned hydrophilic/hydrophobic layers and pinning effects at the pattern edge. *Langmuir* **27**, 3898–3905.
17. Ionov, L., A. Synytska, E. Kaul and S. Diez (2010) Protein-resistant polymer coatings based on surface-adsorbed poly(aminoethyl methacrylate)/poly(ethylene glycol) copolymers. *Biomacromolecules* **11**, 233–237.
18. Imbesi, P. M., N. V. Gohad, M. J. Eller, B. Orihuela, D. Rittschof, E. A. Schweikert, A. S. Mount and K. L. Wooley (2012) Noradrenaline-functionalized hyperbranched fluoropolymer-poly(ethylene glycol) cross-linked networks as dual-mode, anti-biofouling coatings. *ACS Nano* **6**, 1503–1512.
19. Chiag, Y. C., Y. Chang, W. Y. Chen and R. C. Ruaan (2012) Biofouling resistance of ultrafiltration membranes controlled by surface self-assembled coating with PEGylated copolymers. *Langmuir* **28**, 1399–1407.
20. Natalio, F., R. Andre, A. F. Hartog, B. Stoll, K. P. Jochum, R. Wever and W. Tremel (2012) Vanadium pentoxide nanoparticles mimic vanadium haloperoxidases and thwart biofilm formation. *Nat. Nanotechnol.* **7**, 530–535.
21. Krouit, M., R. Granet and P. Krausz (2008) Photobactericidal plastic films based on cellulose esterified by chloroacetate and a cationic porphyrin. *Bioorg. Med. Chem.* **16**, 10091–10097.
22. Li, J., L. Yin, G. Qiu, X. Li, Q. Liu and J. Xie (2015) A photo-bactericidal thin film composite membrane for forward osmosis. *J. Mater. Chem. A* **3**, 6781–6786.
23. Guo, Z., J. Xue, T. Liu, X. Song, Y. Shen and H. Wu (2014) Antibacterial mechanisms of silica/polydopamine/silver nanoparticles against gram positive and gram negative bacteria. *Micro Nano Lett.* **9**, 210–214.
24. Sato, T., Y. Fujimori, T. Nakayama, Y. Gotoh, Y. Sunaga, M. Nemoto, T. Matsunaga and T. Tanaka (2012) Assessment of the anti-biofouling potentials of a copper iodide-doped nylon mesh. *Appl. Microbiol. Biotechnol.* **95**, 1043–1050.
25. Pérez-Roa, R. E., M. A. Anderson, D. Rittschof, C. G. Hunt and D. R. Noguera (2009) Involvement of reactive oxygen species in the electrochemical inhibition of barnacle (*Amphibalanus amphitrite*) settlement. *Biofouling* **25**, 563–571.
26. Zhao, Y., L. Yang, Q. Xu, M. Barahman and A. M. Lyons (2013) Catalytic, self-cleaning surface with stable superhydrophobic properties: Printed polydimethylsiloxane (PDMS) arrays embedded with TiO₂ nanoparticles. *ACS Appl. Mater. Interfaces* **7**, 2632–2640.
27. Busch, T. M., K. A. Cengel and J. C. Finlay (2009) Pheophorbide a as a photosensitizer in photodynamic therapy: In vivo considerations. *Cancer Biol. Ther.* **8**, 540–542.
28. Grossman, C. E., S. Pickup, A. Durham, E. P. Wileyto, M. E. Putt and T. M. Busch (2011) Photodynamic therapy of disseminated non-small cell lung carcinoma in a murine model. *Lasers Surg. Med.* **43**, 663–675.
29. Cerniglia, G. J., S. Dey, S. M. Gallagher-Colombo, N. A. Daurio, S. Tuttle, T. M. Busch, A. Lin, R. Sun, T. V. Eipova, S. A. Vinogradov, N. Denko, C. Koumenis and A. Maity (2015) The PI3K/Akt pathway regulates oxygen metabolism via pyruvate dehydrogenase (PDH)-E1α phosphorylation. *Mol. Cancer Ther.* **14**, 1928–1938.
30. Smith, P. K., R. I. Krohn, G. T. Hermanson, A. K. Mallia, F. H. Gartner, M. D. Provenzano, E. K. Fujimoto, N. M. Goeke, B. J. Olson and D. C. Klenk (1985) Measurement of protein using bicinchoninic acid. *Anal. Biochem.* **150**, 76–85.
31. Wyatt, A. R. and M. R. Wilson (2010) Identification of human plasma proteins as major clients for the extracellular chaperone clusterin. *J. Biol. Chem.* **285**, 3532–3539.
32. McArthur, S. L. (2006) Applications of XPS in bioengineering. *Surf. Interface Anal.* **38**, 1380–1385.

33. Vanea, V. and V. Simon (2013) XPS and Raman study of zinc containing silica microparticles loaded with insulin. *Appl. Surf. Sci.* **280**, 144–150.

34. Bennett, S. M., J. A. Finlay, N. Gunari, D. D. Wells, A. E. Meyer, G. C. Walker, M. E. Callow, J. A. Callow, F. V. Bright and M. R. Detty (2010) The role of surface energy and water wettability in aminoalkyl/fluorocarbon/hydrocarbon-modified xerogel surfaces in the control of marine biofouling. *Biofouling* **26**, 235–246.

35. Sokolova, A., J. J. Bailey, G. T. Waltz, L. H. Brewer, J. A. Finlay, J. Fornalik, D. E. Wendt, M. E. Callow, J. A. Callow, F. V. Bright and M. R. Detty (2012) Spontaneous multiscale phase separation within fluorinated xerogel coatings for fouling-release surfaces. *Biofouling* **28**, 143–157.

36. Hou, X., Y. Hu, A. Grinthal, M. Khan and J. Aizenberg (2015) Liquid-based gating mechanism with tunable multiphase selectivity and antifouling behavior. *Nature* **519**, 70–73.

37. MacCallum, N., C. Howell, P. Kim, D. Sun, R. Friedlander, J. Ranisau, O. Ahanotu, J. J. Lin, A. Vena, B. Hatton, T.-S. Wong and J. Aizenberg (2015) Liquid-infused silicone as a biofouling-free medical material. *ACS Biomater. Sci. Eng.* **1**, 43–51.

38. Rosenhahn, A., S. Schilp, J. Kreuzer and M. Grunze (2010) The role of "inert" surface chemistry in marine biofouling prevention. *Phys. Chem. Chem. Phys.* **12**, 4275–4286.

39. Xiao, L., J. Li, S. Mieszkin, A. Fino, A. Clare, M. Callow, J. Callow, M. Grunze, A. Rosenhahn and P. Levkin (2013) Slippery liquid-infused porous surfaces showing marine antibiofouling properties. *ACS Appl. Mater. Interfaces* **5**, 10074–10080.

40. Xu, Q., Y. Liu, F.-J. Lin, B. Mondal and A. M. Lyons (2013) Superhydrophobic TiO₂–polymer nanocomposite surface with UV-induced reversible wettability and self-cleaning properties. *ACS Appl. Mater. Interfaces* **5**, 8915–8924.

41. Malmsten, M. (1995) Ellipsometry studies of the effects of surface hydrophobicity on protein adsorption. *Colloids Surf. B: Biointerfaces* **3**, 297–308.

42. Iucci, G., G. Polzonetti, G. Infante and L. Rossi (2004) XPS and FT-IR spectroscopy study of albumin adsorption on the surface of a π-conjugated polymer film. *Surf. Interface Anal.* **36**, 724–728.

43. Gruian, C., E. Vanea, S. Simon and V. Simon (2012) FTIR and XPS studies of protein adsorption onto functionalized bioactive glass. *Biochim. Biophys. Acta* **1824**, 873–881.

44. Vanea, E. and V. Simon (2011) XPS study of protein adsorption onto nanocrystalline aluminosilicate microparticles. *Appl. Surf. Sci.* **257**, 2346–2352.

45. Zander, N., J. A. Orlicki, A. M. Rawlett and T. P. Beebe (2012) Quantification of protein incorporated into electrospun polycaprolactone tissue engineering scaffolds. *ACS Appl. Mater. Interfaces* **4**, 2074–2081.

46. McUmber, A., T. Randolph and D. Schwartz (2015) Electrostatic interactions influence protein adsorption (but not desorption) at the silica–aqueous interface. *J. Phys. Chem. Lett.* **6**, 2583–2587.

47. Moerz, S. and P. Huber (2014) Protein adsorption into mesopores: A combination of electrostatic interaction, counterion release, and van der Waals forces. *Langmuir* **30**, 2729–2737.

48. Prime, K. L. and G. M. Whitesides (1995) Spacer groups (PEG moieties) with as low as three ethylene glycol repeating units have been shown to essentially eliminate electrostatic attractions. *J. Am. Chem. Soc.* **115**, 10714–10721.

49. Xu, N., M. Yao, W. Farinelli, Z. Hajjarian, Y. Wang, R. W. Redmond and I. E. Kochevar (2015) Light-activated sealing of skin wounds. *Lasers Surg. Med.* **47**, 17–29.

50. Yao, M., A. Yaroslavsky, F. P. Henry, R. W. Redmond and I. E. Kochevar (2010) Phototoxicity is not associated with photochemical tissue bonding of skin. *Lasers Surg. Med.* **42**, 123–131.

51. Miñán, A., C. Lorente, A. Ipiña, A. H. Thomas, M. Fernández Lorenzo de Mele and P. L. Schilardi (2015) Photodynamic inactivation induced by carboxypterin: A novel non-toxic bactericidal strategy against planktonic cells and biofilms of *Staphylococcus aureus*. *Biofouling* **31**, 459–468.

52. Takemura, T., N. Ohta, S. Nakajima and I. Sakata (1992) The mechanism of photosensitization in photodynamic therapy: Chemiluminescence caused by photosensitization of porphyrins in saline containing human serum albumin. *Photochem. Photobiol.* **55**, 137–140.

53. Alarcón, E., A. M. Edwards, A. M. Garcia, A. Muñoz, A. Aspée, C. D. Borsarelli and E. A. Lissi (2009) Photophysics and photochemistry of zinc phthalocyanine/bovine serum albumin adducts. *Photochem. Photobiol. Sci.* **8**, 255–263.

54. Ferraz, R. C., C. R. Fontana, A. P. Ribeiro, F. Z. Trindade, F. H. Bartoloni, J. W. Baader, E. C. Lins, V. S. Bagnato and C. Kurachi (2011) Chemiluminescence as a PDT light source for microbial control. *J. Photochem. Photobiol., B* **103**, 87–92.

55. Mano, C. M., F. M. Prado, J. Massari, G. E. Ronsein, G. R. Martinez, S. Miyamoto, J. Cadet, H. Sies, M. H. G. Medeiros, E. J. H. Bechara and P. Di Mascio (2014) Excited singlet molecular O₂ (¹Δ_g) is generated enzymatically from excited carbonyls in the dark. *Sci. Rep.* **4**, 5938.

56. Miyamoto, S., G. R. Martinez, M. H. Medeiros and P. Di Mascio (2014) Singlet molecular oxygen generated by biological hydroperoxides. *J. Photochem. Photobiol., B* **139**, 24–33.

57. Choi, C.-H. and C.-J. Kim (2009) Droplet evaporation of pure water and protein solution on nanostructured superhydrophobic surfaces of varying heights. *Langmuir* **25**, 7561–7567.

58. Lima, A. C. and J. F. Mano (2015) Micro/nano-structured superhydrophobic surfaces in the biomedical field: Part II: applications overview. *Nanomedicine* **10**, 271–297.

59. Kuthanapillil, J., R. R. Avirah and D. Ramaiah (2007) Development of squaraine dyes for photodynamic therapeutical applications: Synthesis and study of electronic factors in the dye formation reaction. *ARKIVOC* **8**, 296–310.

60. Shimshon, B. D., I. Bronshtein, Y. Garini, W. G. O'Neal, P. A. Jacobi and B. Ehrenberg (2009) The localization and photosensitization of modified chlorin photosensitizers in artificial membranes. *Photochem. Photobiol. Sci.* **8**, 354–361.

61. Shimshon, B. D., I. Bronshtein, A. Wiehe, B. Roder, M. O. Senge and B. Ehrenberg (2006) On the correlation between hydrophobicity, liposome binding and cellular uptake of porphyrin sensitizers. *Photochem. Photobiol.* **82**, 695–701.

62. Dosselli, R., R. Ruiz-Gonzalez, F. Moret, V. Agnolon, C. Compagnin, M. Mognato, V. Sella, M. Agut, S. Nonell, M. Gobbo and E. Reddi (2014) Synthesis, spectroscopic, and photophysical characterization and photosensitizing activity toward prokaryotic and eukaryotic cells of porphyrin-magainin and -buforin conjugates. *J. Med. Chem.* **57**, 1403–1415.

63. Jux, N. and Röder B. (2010) Targeting strategies for tetrapyrrole-based photodynamic therapy. In *Handbook of Porphyrin Science*, Vol. 4 (Edited by K. M. Kadish, K. M. Smith and R. Guilard), pp. 325–401. World Scientific Publishing Co. Pte. Ltd., Singapore.

64. Majumdar, P., R. Nomula and J. Zhao (2014) Activatable triplet photosensitizers: Magic bullets for targeted photodynamic therapy. *J. Mater. Chem. C* **2**, 5982–5997.

65. Zhao, J., W. Wu, J. Sun and S. Guo (2013) Triplet photosensitizers: From molecular design to applications. *Chem. Soc. Rev.* **42**, 5323–5351.

66. Agostinis, P., K. Berg, K. A. Cengel, T. H. Foster, A. W. Girotti, S. O. Gollnick, S. M. Hahn, M. R. Hamblin, A. Juzeniene, D. Kessel, M. Korbelik, J. Moan, P. Mroz, D. Nowis, J. Piette, B. C. Wilson and J. Golab (2011) Photodynamic therapy of cancer: An update. *CA Cancer J. Clin.* **61**, 250–281.

67. St. Denis, T. G., Y.-Y. Huang and M. R. Hamblin (2014) Cyclic tetrapyrroles in photodynamic therapy: the chemistry of porphyrins and related compounds in medicine. In *Handbook of Porphyrin Science*, Vol. 27 (Edited by K. M. Kadish, K. M. Smith and R. Guilard), pp. 255–301. World Scientific Publishing Co. Pte. Ltd., Singapore.

68. Dąbrowski, J. M. and L. G. Arnaut (2015) Photodynamic therapy (PDT) of cancer: From local to systemic treatment. *Photochem. Photobiol. Sci.* **14**, 1765–1780.